Experimental Investigation of Air-Sea Transfer of Momentum and Enthalpy at High Wind Speed

By: Moshe Alamaro[1], Kerry A. Emanuel[1], Wade R. McGillis[2]

[1] *Department of Earth, Atmospheric and Planetary Sciences, Massachusetts Institute of Technology;* [2] *Woods Holes Oceanographic Institution.*

Abstract. Thermodynamic analysis and numerical modeling of hurricanes show that their intensity is sensitive to enthalpy and momentum transfer from the ocean surface. Since direct measurements of drag are not easily performed on the high seas, an annular wind-wave tank was constructed to simulate some aspects of the tropical storm boundary layer. The maximum air velocity inside the annular tank is comparable to that of a hurricane.

This paper describes the design and engineering of the tank, the fluid mechanics of the rotational flow in the tank using angular momentum analysis, the design of the experiments, and experimental results. It provides experimental data on drag and latent enthalpy transfer at high air speed relative to the moving water surface. The design of the wind-wave tank and the experiments provide a foundation for future and more comprehensive high air speed experimental programs using a linear tank.

Key Words: Air-sea interaction, spray, tropical cyclones, heat and momentum transfer.

1. Introduction

Basic theory (e.g., Emanuel 1986) and numerical experiments (Ooyama 1969; Rosenthal 1971; Emanuel 1995a) show that the intensity of tropical cyclones depends strongly on the coefficients for the transfers of momentum (C_D) and enthalpy (C_k) between the ocean and the atmospheric boundary layer. The maximum wind speed, in particular, depends on $(C_k / C_D)^{1/2}$ in the high wind speed core of the storm (Emanuel 1986). Unfortunately, there are no simultaneous measurements of the effective values of these coefficients at wind speeds greater than about 25 m s^{-1}, and the theory of air–sea interaction at very high wind speeds is poorly developed. The agitated sea no doubt increases the effective roughness length and, thereby, C_D and the dissipation rate of kinetic energy; while, for wind speeds up to about 20 m s^{-1}, there is little observational

evidence to suggest a corresponding increase in C_k (Geernaert et al. 1987). Emanuel (1995a) showed that if estimated values of the exchange coefficients at 20 m s^{-1} are applied at higher wind speeds, maintaining a storm of much greater than marginal hurricane intensity would be impossible. Some mechanism must also serve to enhance air–sea enthalpy exchange at high wind speed.

Given the many obstacles to obtaining field measurements at hurricane wind speeds, we have attempted to make progress by performing a series of experiments in an annular wind-wave flume of our own design. While the geometry of the tank places serious limitations on scaling our results up to the real ocean-atmosphere system, it allows us to make quite precise estimates of exchange coefficients. Our estimates of the drag coefficient are broadly consistent with the recent work of Powell et al. (2003) and Donelan et al. (2004), and we believe that our methodology can be applied to the design and execution of experiments in larger tanks. To our knowledge, our results represent the first quantitative experimental deductions of enthalpy fluxes at hurricane wind speeds.

2. Experimental Apparatus

A circular wind wave tank made of two acrylic concentric walls was constructed, as shown in Figures 1 and 2. A rotor, powered by a 1 kW electric motor, moves the air over the water surface and the shear stress propels the water around the tank. An Acoustic Doppler Velocitmeter (ADV) measures the water velocity and an anemometer measures the air velocity. The tank is equipped with an adjustable false bottom that enables the distance from the rotor to the water surface to be varied for the same depth of water. The tank is also equipped to conduct enthalpy transfer experiments. All the experiments used Poland Spring™ water to minimize variations in water properties.

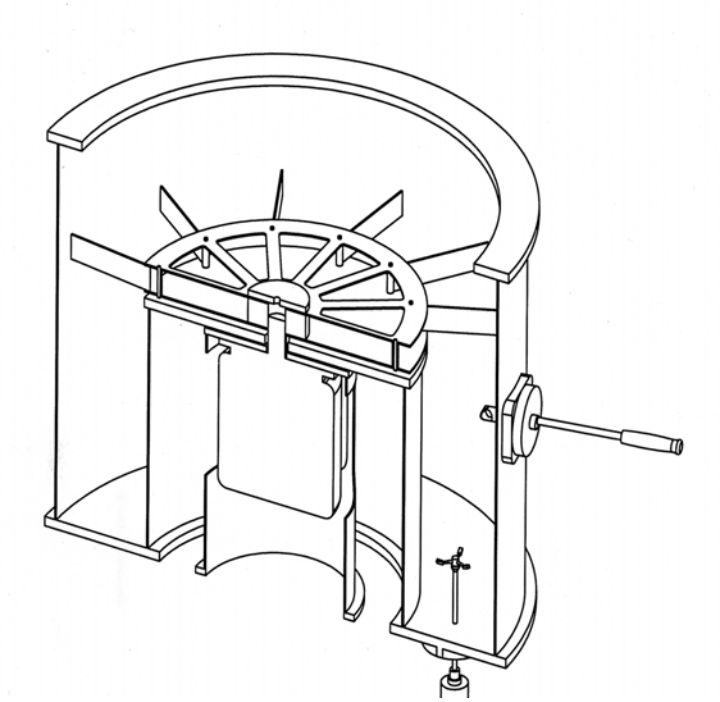

Figure 1: 3-D view of the annular wind wave tank. The outer and inner radiuses are $r_0 = 0.479\ m$ and $r_{in} = 0.284\ m$ respectively.

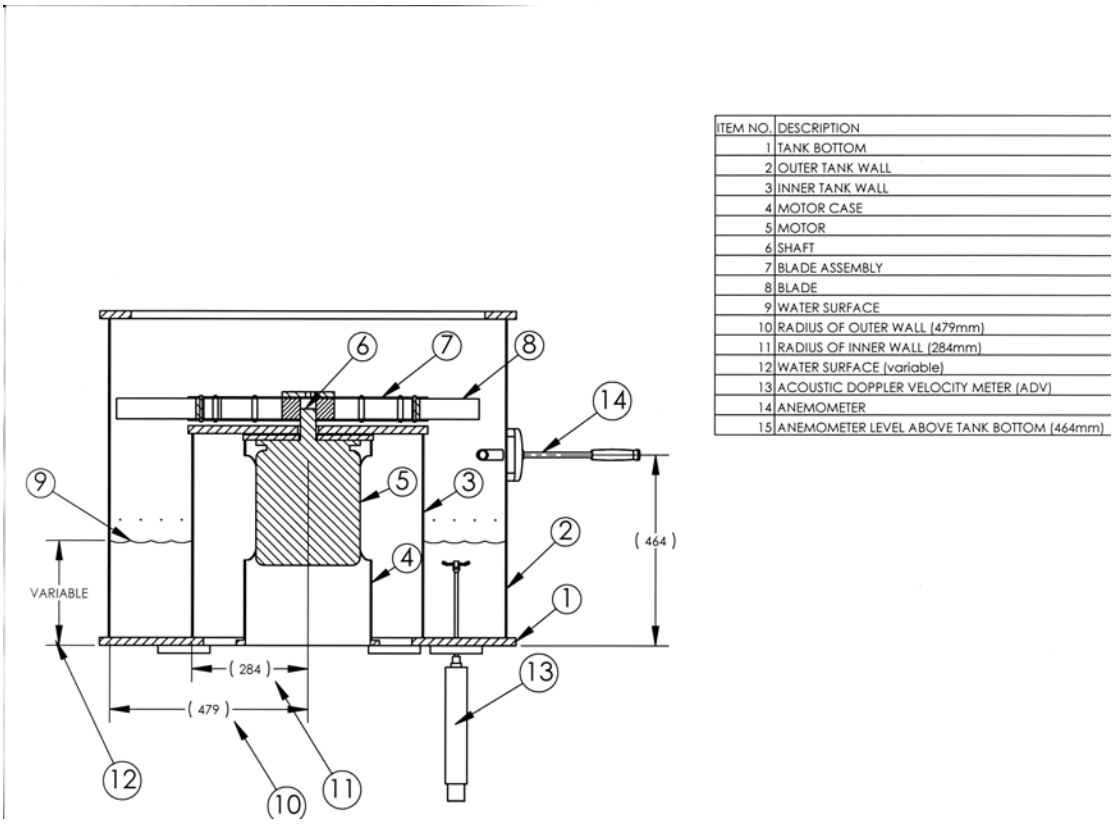

ITEM NO.	DESCRIPTION
1	TANK BOTTOM
2	OUTER TANK WALL
3	INNER TANK WALL
4	MOTOR CASE
5	MOTOR
6	SHAFT
7	BLADE ASSEMBLY
8	BLADE
9	WATER SURFACE
10	RADIUS OF OUTER WALL (479mm)
11	RADIUS OF INNER WALL (284mm)
12	WATER SURFACE (variable)
13	ACOUSTIC DOPPLER VELOCITY METER (ADV)
14	ANEMOMETER
15	ANEMOMETER LEVEL ABOVE TANK BOTTOM (464mm)

Figure 2: Cross section of wind wave tank and dimensions in mm.

3. Angular momentum and shear stress analysis

3.1 Basic Formulation

The drag coefficient over the ocean surface is defined as:

$$C_D = \frac{\tau_s}{\rho_a V_{10}^2} \tag{1}$$

Where τ_s is the shear stress over the water surface, ρ_a is the air density and V_{10} is the air velocity relative to the water at a reference height of 10 meters. The following is a simplified model that enables the simulation, measurement, and calculation of the shear stress τ_s over the water surface in the wind wave tank. The model uses angular momentum equations for the rotating water mass. Given that the water has no density stratification, Ekman pumping quickly communicates surface and wall stresses to the interior, allowing us to approximate the motion outside the boundary layers as solid body rotation.

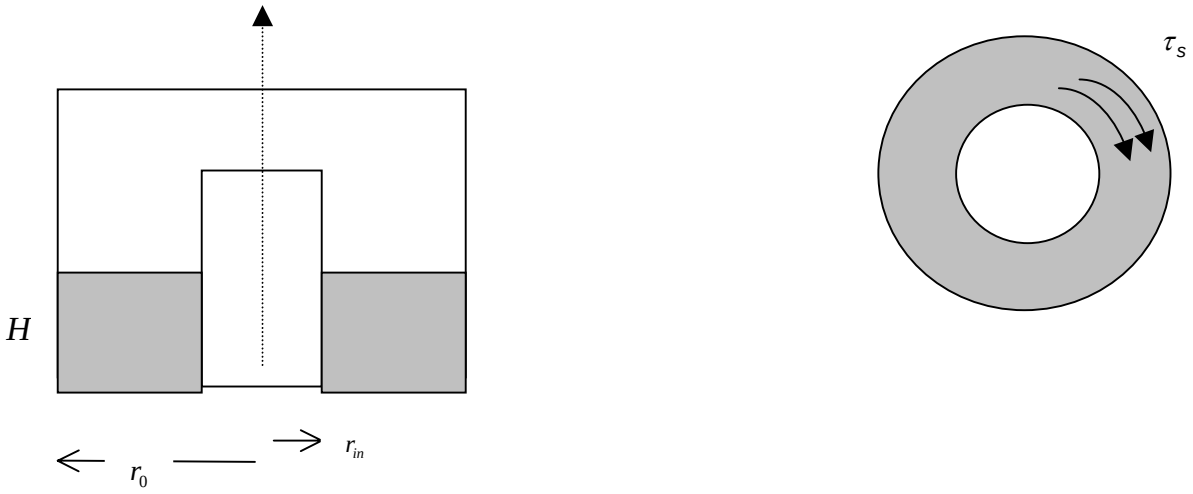

Figure 3: Side and upper views of the wind wave tank. Air motion over the water surface results in a propelling shear stress τ_s and propelling torque T_{propel}.

We further approximate the radial varying shear stress by a suitably defined radial mean value. The differential propelling torque provided by the stress applied to a differential water surface area $dA = r d\theta \cdot dr$ is:

$$dT_{propel} = \tau_s dA\, r \tag{2}$$

The entire propelling torque is:

$$T_{propel} = \int_{r_{in}}^{r_0} \int_0^{2\pi} \tau_s dA\, r = \int_{r_{in}}^{r_0} \int_0^{2\pi} \tau_s r d\theta \cdot dr\, r = \frac{2}{3}\pi\left(r_0^3 - r_{in}^3\right) \cdot \tau_s \tag{3}$$

The outer, inner, and bottom walls provide a retarding torque T_{retard} through shear stresses. The total torque on the rigid body rotating water mass is then:

$$T_{total} = T_{propel} + T_{retard} \tag{4}$$

The angular momentum of a differential water mass, assuming rigid body rotation with angular velocity Ω, is:

$$dM = \rho_w \; (r\, d\theta\, dr\, dz)\, (\Omega r)\, r \tag{5}$$

where ρ_w is the water density. Assuming thin boundary layers, the total angular momentum of the water mass is thus

$$M = \rho_w \int_0^H dz \int_0^{2\pi} d\theta \int_{r_{in}}^{r_0} r^3 dr = \frac{\pi}{2} \rho_w H\left(r_0^4 - r_{in}^4\right)\Omega \tag{6}$$

where H is the water depth. To derive an angular motion equation, we use the fact that the rate of change of the angular momentum is equal to the total applied torque:

$$\frac{\partial M}{\partial t} = \frac{\pi}{2}\rho_w H\left(r_0^4 - r_{in}^4\right)\frac{\partial \Omega}{\partial t} = T_{propel} + T_{retard} \tag{7}$$

In the steady state: $\frac{\partial M}{\partial t} = 0$ and $T_{propel} = -T_{retard}$ (8)

3.2 Propelling torque and stress

The procedure for measuring and calculating the propelling torque and stress is as follows: First bring the water mass to a steady state rotation for certain V_s - the relative air velocity over the moving water surface. Then abruptly switch off the electric motor, removing the surface wind stress. The equation of motion just after the stress vanishes, at $t = 0$, is:

$$\frac{\partial M}{\partial t} = \frac{1}{2}\pi\rho_w H\left(r_0^4 - r_{in}^4\right)\frac{\partial \Omega}{\partial t} = -T_{retard} = +T_{propel} \quad (9)$$

Measuring $\frac{\partial \Omega}{\partial t}$ just after spindown starts thus enables us to determine the propelling torque and the propelling shear stress just before spindown. By combining (9) with (3) we get:

$$T_{propel} = \frac{2}{3}\pi\left(r_0^3 - r_{in}^3\right)\cdot \tau_s = -\frac{1}{2}\pi\rho_w H\left(r_0^4 - r_{in}^4\right)\frac{\partial \Omega}{\partial t} = I_w \cdot \frac{\partial \Omega}{\partial t} \quad (10)$$

Where I_w is the moment of inertia of the water mass defined as:

$$I_w = \frac{1}{2}\pi\rho_w H\left(r_0^4 - r_{in}^4\right) \quad (11)$$

and the surface shear stress is:

$$\tau_s = -\frac{\frac{1}{2}\pi\rho_w H\left(r_0^4 - r_{in}^4\right)\frac{\partial \Omega}{\partial t}}{\frac{2}{3}\pi\left(r_0^3 - r_{in}^3\right)} = -\frac{3}{4}\rho_w H\frac{\left(r_0^4 - r_{in}^4\right)}{\left(r_0^3 - r_{in}^3\right)}\frac{\partial \Omega}{\partial t} \quad (12)$$

To obtain $\frac{\partial \Omega}{\partial t}$ of the water mass, the velocity of the water V_w is measured at a distance R_D (the location of the ADV) from the tank center so that: $\frac{\partial \Omega}{\partial t} = \frac{1}{R_D}\frac{\partial V_w}{\partial t}$.
Substituting into (11):

$$\tau_s = -\frac{3}{4}\rho_w \frac{H}{R_D}\frac{\left(r_0^4 - r_{in}^4\right)}{\left(r_0^3 - r_{in}^3\right)}\frac{\partial V_w}{\partial t} \qquad (13)$$

The deceleration of the water mass $\frac{\partial V_w}{\partial t}$ is obtained by spindown experiments that are described in later sections. The surface area over which the stress acts is corrected for curvature of the water surface, as described in the Appendix.

4. Fluid mechanics of rotational water and air and spindown experiments

4.1 Spindown formulation

The spindown technique is central to this investigation. It provides information on the deceleration of the water mass that in turn enables the calculation of the shear stress on the water surface. The experiment is compromised by surface waves and inertial oscillations that cause irregular tangential velocity, and Ekman flows of both the water and the air cause departures from solid body rotation. Instrument noise also introduces uncertainties.

We hypothesize that the water flow in the tank can be modeled as a channel flow. This flow has a velocity V_w on the order of 0.5 m/sec, and hydraulic diameter D_h on the order of 0.2 m. Therefore, the Reynolds number of the water flow

is about: $R_e = \frac{V_w D_h}{\nu_w} = \frac{0.5 \cdot 0.2}{10^{-6}} \approx 10^5$ Therefore we expect the flow to be turbulent.

For channel and pipe flow, a “friction factor” f is defined which is measured for the head or pressure losses due to shear stresses on the walls. For laminar pipe flow f has an

analytical expression while for turbulent channel and pipe flows semi empirical expressions are used. For both turbulent and laminar channel and pipe flows, the friction factor f is always a decreasing function of $\boldsymbol{R_e}$. This is shown graphically by the Moody Chart (Fox, 1998). Semi empirical formulas provide correlations for $f(R_e)$ for various ranges of $\boldsymbol{R_e}$. For example, the Blasius correlation gives (Fox, 1998):

$$\boldsymbol{f = 4C_f = \frac{0.316}{R_e^{0.25}}} \qquad \text{for } \boldsymbol{R_e \le 10^5} \tag{14}$$

Here $\boldsymbol{C_f}$ is the coefficient we use to relate the spindown of the water mass to the tank wall stress. (It is not the drag coefficient between the water surface and the airflow.) According to the Moody Chart and the Blasius correlation, for turbulent or laminar flow, $\boldsymbol{C_f}$ or $\boldsymbol{C_{DW}}$ is a decreasing function of $\boldsymbol{R_e}$ for all values of $\boldsymbol{R_e}$.

The ODE describing the spindown is:

$$\boldsymbol{I_w \cdot \frac{d\Omega}{dt} = I_w \cdot \frac{1}{R_D}\frac{dV_w}{dt} = -A\rho_w C_{DW} \cdot V_{wo}^2 \cdot r_0} \tag{15}$$

where $\boldsymbol{I_w}$ is the moment of inertia of the water mass defined in (11), $\boldsymbol{V_{wo}}$ is the water velocity on the outer wall (when we ignore the thickness of boundary layer on the outer wall) and $\boldsymbol{r_o}$ is the radius of the outer wall.

The assumption of rigid body rotation of the water mass gives:

$$\boldsymbol{\left(\frac{V_{wo}}{V_w}\right)^2 = \left(\frac{r_0}{R_D}\right)^2} \tag{16}$$

where $\boldsymbol{R_D}$ is the distance of the ADV from the tank center where the water velocity $\boldsymbol{V_w}$ is measured.

Substituting the expression for the moment of inertia given in (11) and equation (16) into equation (15):

$$\frac{\partial V_w}{\partial t} = -k_1 C_{Dw} \cdot V_w^2 \tag{17}$$

Where $K_1 = \frac{A}{I_w}\frac{r_o^3}{R_D}\rho_w$ is a constant for a specific experiment the dimension of which is $[m^{-1}]$.

Assume that for a turbulent flow, C_{DW} is a power function of the Reynolds number as shown by the Blasius equation, or equivalently, a power function of the water velocity:

$$C_{DW} \propto R_e^x \propto V_w{}^x \tag{18}$$

where x is any number. Substituting (18) into (17):

$$\frac{dV_w}{dt} = -k \;\; V_w{}^{2+x} \tag{19}$$

Solving this last ODE:

$$V_w(t) = \frac{V_m}{(1+k\cdot t)^{\frac{1}{1+x}}} = \frac{V_m}{(1+k\cdot t)^n} \tag{20}$$

Where $n = \frac{1}{1+x}$, V_m is the water velocity at $t = 0$ and k is some constant. Also:

$$x = \frac{1-n}{n} \tag{21}$$

For x to be negative as required by the Blasius correlation or by the Moody Chart, it is required that $n > 1$.

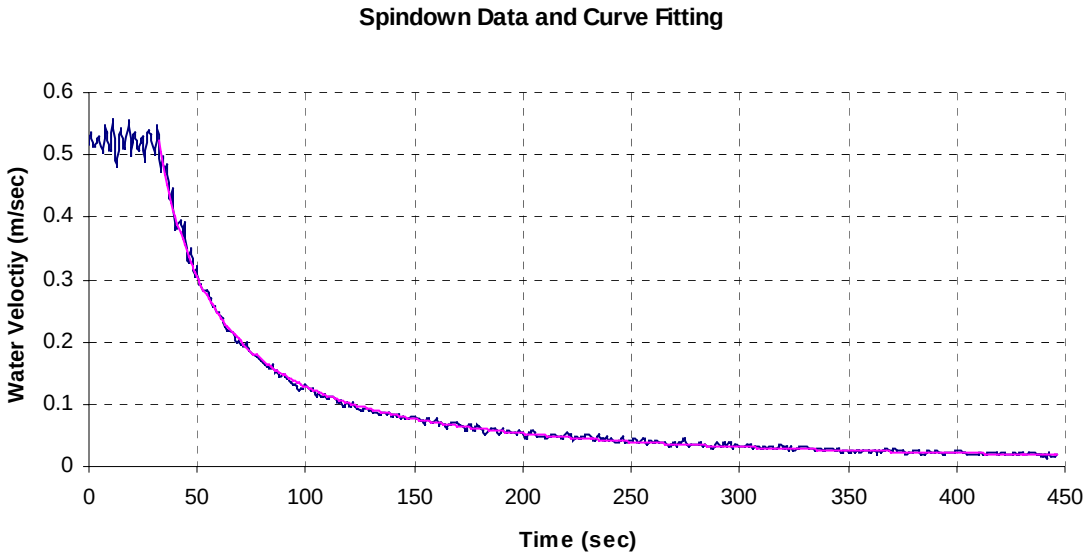

Figure 4: Spindown date and curve fitting done by Excel.

Figure 4 shows an example of spindown data and a curve fit to the data. For this particular experiment, curve fitting gives:

$$V_w(t) = \frac{0.5222}{(1 + 0.0028562 * t)^{1.3014}} \tag{22}$$

In eq. (22) $t = 0$ is the beginning of the spindown shown in Figure 3. Repeating the same spindown experiment a few times, different pairs of n and k are obtained simultaneously for each experiment.

4.2 The derivative of water velocity

Once the coefficients n and k have been obtained for each spindown experiment, the time derivative of (20) is used to estimate the shear stress by applying equation (13). The general form of the curve fitting formula is:

$$V_w(t) = \frac{V_m}{(1 + k \cdot t)^n} \tag{23}$$

Differentiation gives:

$$\frac{\partial V_w}{\partial t} = \frac{-nkV_m}{(1+k\cdot t)^{n+1}} = \frac{-nkV_w}{(1+k\cdot t)} = -nkV_w\left(\frac{V_w}{V_m}\right)^{\frac{1}{n}} \tag{24}$$

This expression has been used in (13) to calculate the shear stress.

5. The drag experiments: analysis and results

This section outlines, step-by-step, the procedure for the drag experiments, their analysis and results for drag coefficients. The following figures are shown for experiments that used a 14 cm water depth since for this water depth the ADV could measure the water velocity in the middle of the water column. Also, this depth of water was not so great as to substantially reduce the maximum RPM for the given electric motor power. Experiments were done once with the lid on to enable high RPM and air speed and once with the lid off to enable evaporation and enthalpy transfer from the tank to the ambient laboratory. The lid-off drag experiments reached a maximum RPM of 560 while the lid-off enthalpy experiments reached a maximum of 480 RPM. The lid-on drag experiments, however, reached 760 RPM. This is because, without the lid, the electric motor must not only do work against frictional dissipation in the apparatus, but must also accelerate ambient air that is continually exchanged through the top. Also, in the evaporation experiments, heating elements were submerged in the water, obstructing its flow and causing the maximum RPM to be lower than in the tank without heating elements.

The experimental procedure is as follows:

a. The steady-state water velocity is measured vs. paddle RPM. The lowest RPM is 40 and the highest for a tank covered with a lid is about 760, depending on the amount of water in the tank. The RPM was changed by increments of 20. At low RPM, the time necessary to bring the water to steady state is long and it is generally shorter for higher RPM. For an intermediate 200-400 RPM, the necessary time is about 2 minutes. For the lowest 40 RPM the time can be as long as 7-10 minutes.

b. Once the water velocity reaches steady state, the water velocity is recorded for 30-60 seconds and is averaged for each RPM.

c. Air speed is measured as a function of RPM by an anemometer at a fixed height above the water surface and is shown in Figure 6. The water speed for a specific RPM is subtracted from the air speed to obtain the relative air velocity over the water surface. Since relative air speed is known as a function of RPM and all other data is given as a function of RPM, all other data can be calculated as a function of relative air speed. It was observed that the air speed strongly affects the water speed and wave pattern but water depth, speed and wave patterns do not significantly affect the air speed.

d. The spindown and curve fitting procedures described in section 4 are performed in order to calculate the coefficients ***n*** and ***k*** governing the decelerating water velocity as given by eq. (23). These values are used in eq. (24) to calculate the time derivative of the velocity.

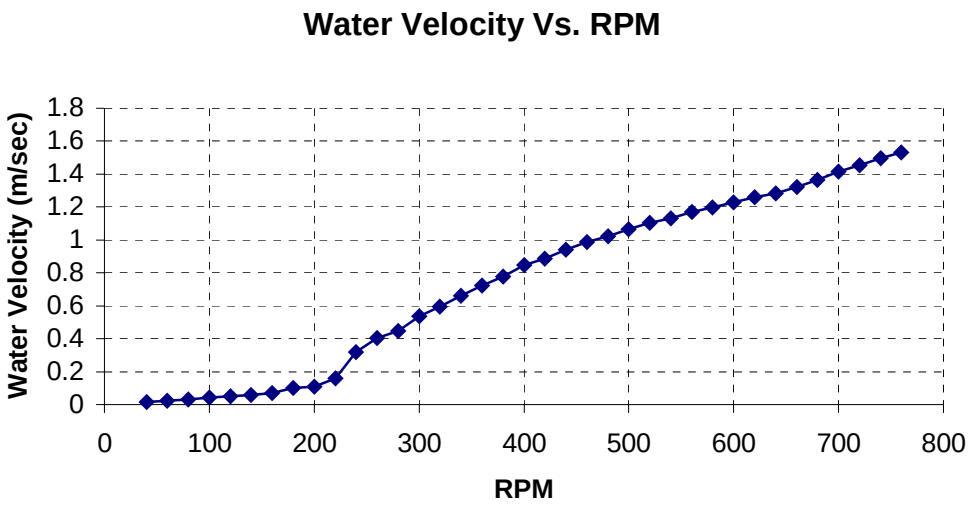

Figure 5: Water velocity vs. RPM. Around 220-280 RPM the surface becomes rough, resulting in wave drag and a marked increase in the slope of water velocity vs. RPM.

The derivative is used in eq. (13) to calculate the shear stress τ_{pf} over the parabolic water surface (see appendix). The friction velocity is obtained using:

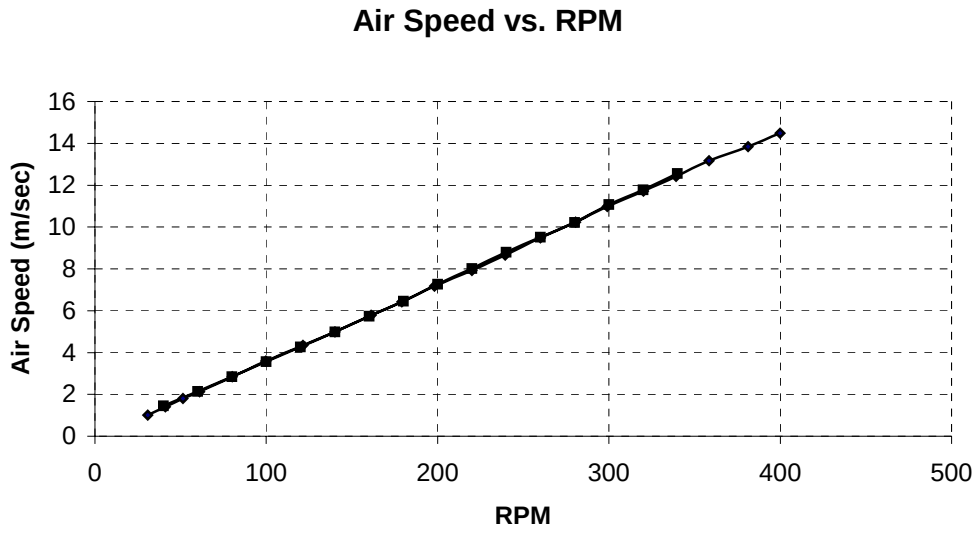

Figure 6: Air speed vs. RPM for two experiments. The water surface in the first is 25 cm and in the second is 12 cm above tank bottom. The air speed vs. RPM is approximately equal for the two experiments.

$$u_* = \sqrt{\frac{\tau_{pf}}{\rho_a}} \tag{25}$$

where ρ_a is the air density.

The drag coefficient is calculated by assuming that the wind velocity has a logarithmic profile and extrapolating it to 10 m height. An intermediate step is the calculation of the "roughness" of the water surface. The expression used to calculate the roughness is:

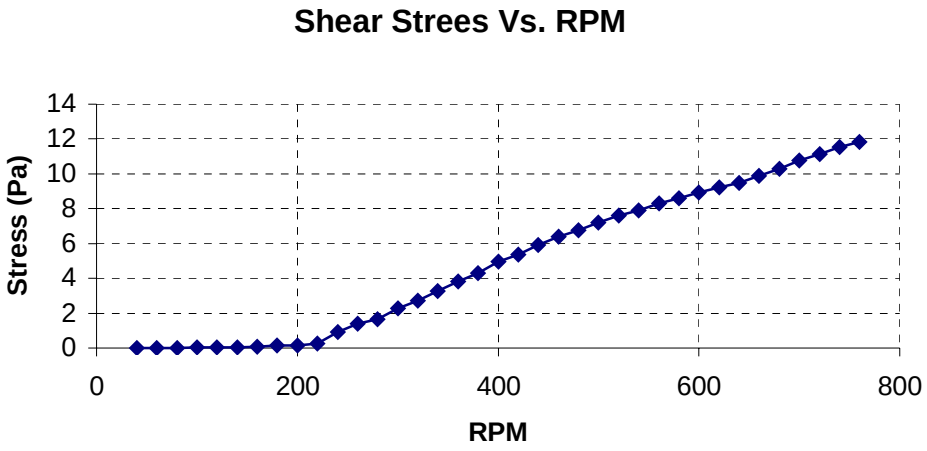

Figure 7: Typical Shear stress vs. RPM

$$\frac{u_a}{u_*} = \frac{1}{k}\ln\left(\frac{z_a}{z_0}\right) \tag{26}$$

where u_a is the relative air velocity over the water surface, measured at height z_a, and

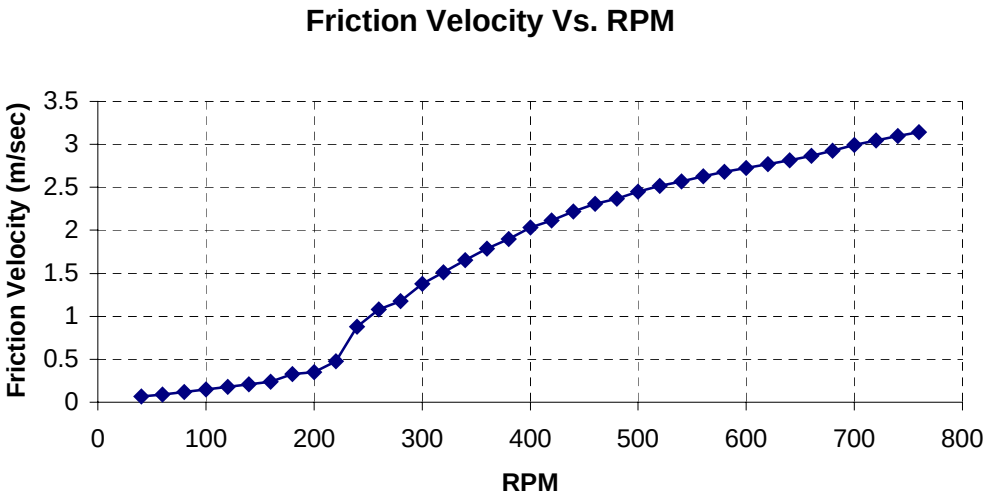

Figure 8: Typical friction velocity vs. RPM

$k = 0.41$ is the Von Karman coefficient. The anemometer was placed at $0.425\ m$ above the tank bottom where the water surface height measured from the bottom of the tank is H. The expression for z_a is:

$$z_a = 0.425 - H \tag{27}$$

Equation (27) enables the calculation of the roughness:

$$z_0 = z_a \cdot \exp\left(-k\frac{u_a}{u_*}\right) \tag{28}$$

The air velocity at a height of 10 m above the water surface is found by (28) and (26):

$$U_{10} = \frac{u_*}{k}\ln\left(\frac{10}{z_0}\right) \tag{29}$$

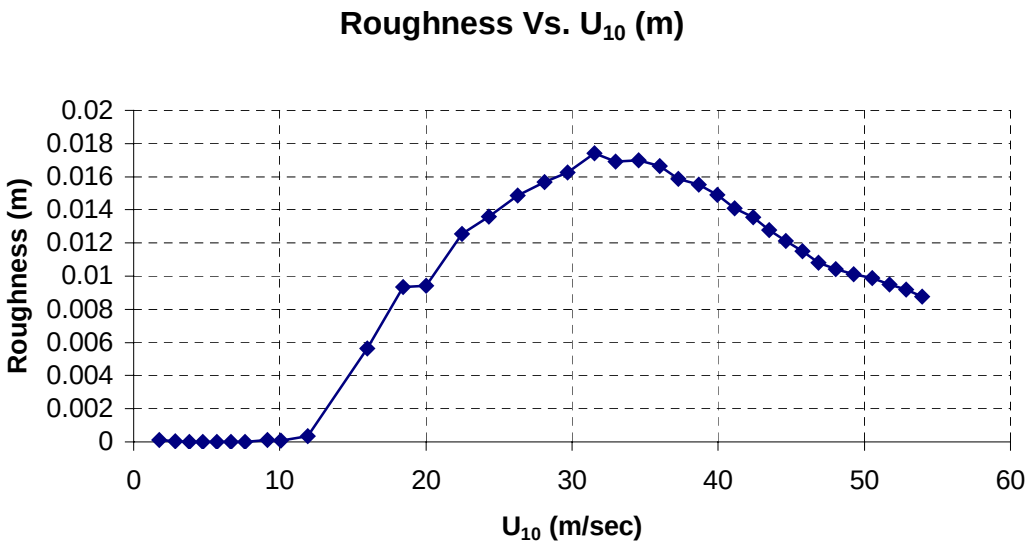

Figure 9: Roughness length in meters vs. U_{10}, the extrapolated air speed 10 meters above the water surface. The calculated "unphysical" roughness length range is 0-20 mm.

The non-dimensional drag coefficient is obtained by dividing the shear stress by the dynamic pressure at the reference air velocity $\boldsymbol{U_{10}}$ obtained in (29). The drag coefficient is:

$$\boldsymbol{C_{D_{10}}} = \frac{\tau_s}{\rho_a U_{10}^2} = \left(\frac{u_*}{U_{10}}\right)^2 \tag{30}$$

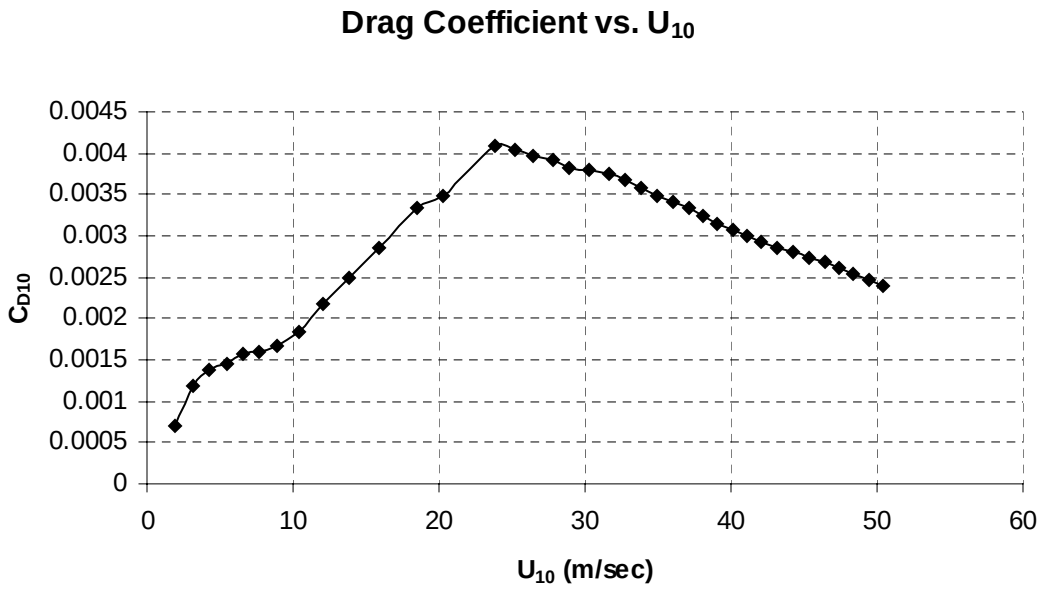

Figure 10: Drag coefficient vs. the extrapolated wind speed at a height of 10 meters above the water surface.

The results for the drag coefficient vs. $\boldsymbol{U_{10}}$ shown in Figure 10 are consistent with those of Donealn (2004) who used momentum budget showing a steep increase in the drag coefficient up to a wind speed of 25-30 m/sec and then leveling and a decrease of the drag coefficient for a wind speed higher than 30 m/sec. This steep increase and leveling of the drag coefficient is also consistent with recent deductions from dropwindsondes deployed in hurricanes Powell (2003), although the highest C_{D10} in Donealn's work is 2.5 10^{-3} while our is 4.0 10^{-3} for air speed of 25-30 m/sec.

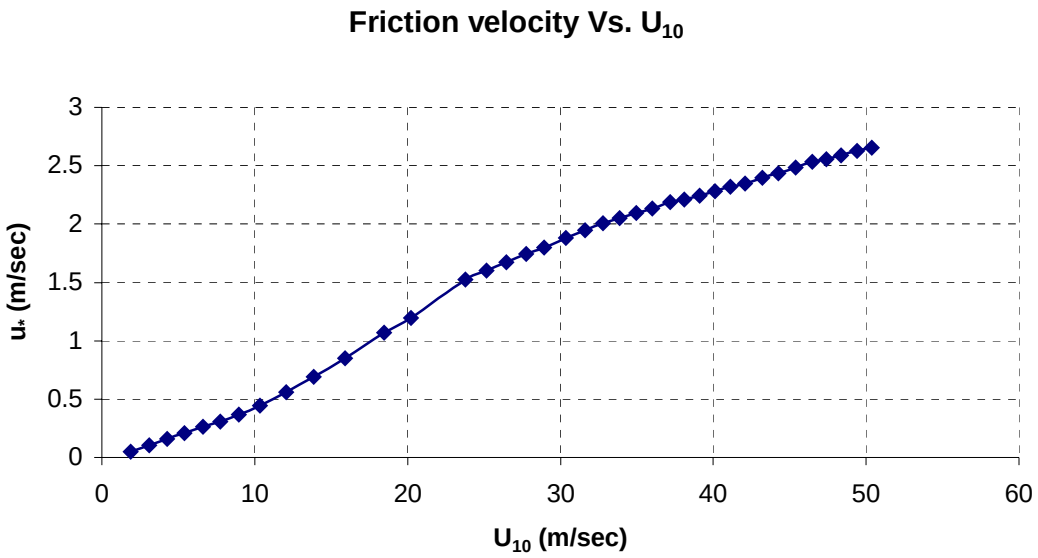

Figure 11: Friction velocity vs. the extrapolated wind speed at a height of 10 meters above the water surface.

The data in Figures 10 and 12 will be used later on to normalize the enthalpy transfer coefficient with U_{10}.

6. Enthalpy Transfer Experiments

6.1 Introduction and experimental apparatus

A schematic drawing for the tank equipped and modified for the enthalpy transfer experiment is shown in figure 12. Submerged heating elements are powered using a 20 Volt transformer. During the experiments, the paddle moves the air over the water, and the air motion enhances the enthalpy transfer from the water into the lab ambient environment. Humidity and temperature sensors were placed in the room and this information was fed into a Program Logic Controller (PLC). A thermocouple measures the bulk temperature of the water in the tank and this information is also fed into the PLC. The PLC controls the on-off power input into the heating elements so the water temperature is kept equal (within a margin of 0.2 C) to the lab ambient temperature. In this way, heat transfer from the room into the tank through the tank walls is minimized.

The water level in the tank during all the enthalpy transfer experiments was 14 cm. This water height, which was also used for the drag experiments, gave consistent results. Each experiment was conducted using Poland Springs^{TM} water and the water was always changed after each experiment. Each experiment was conducted over 24-48 hours. The surface tension of the water was measured before and after an experiment and was found to be constant, having a value of 75-80 dyne/cm.

The water in the tank was connected by a pipe to an external cup so the water levels in the tank and the cup are equal. A needle attached to a micrometer is used to gauge the water level in the cup before and after the experiment, measuring the water loss during the experiment. The water level in the tank during the experiment was kept at $\mathbf{14 \pm 1}\boldsymbol{cm}$. If necessary, the experiment was briefly interrupted and a known amount of water was added. Each experiment was done for a specific RPM. Air velocity vs. RPM was measured using an anemometer at a specified height above the water surface, as in the drag experiments.

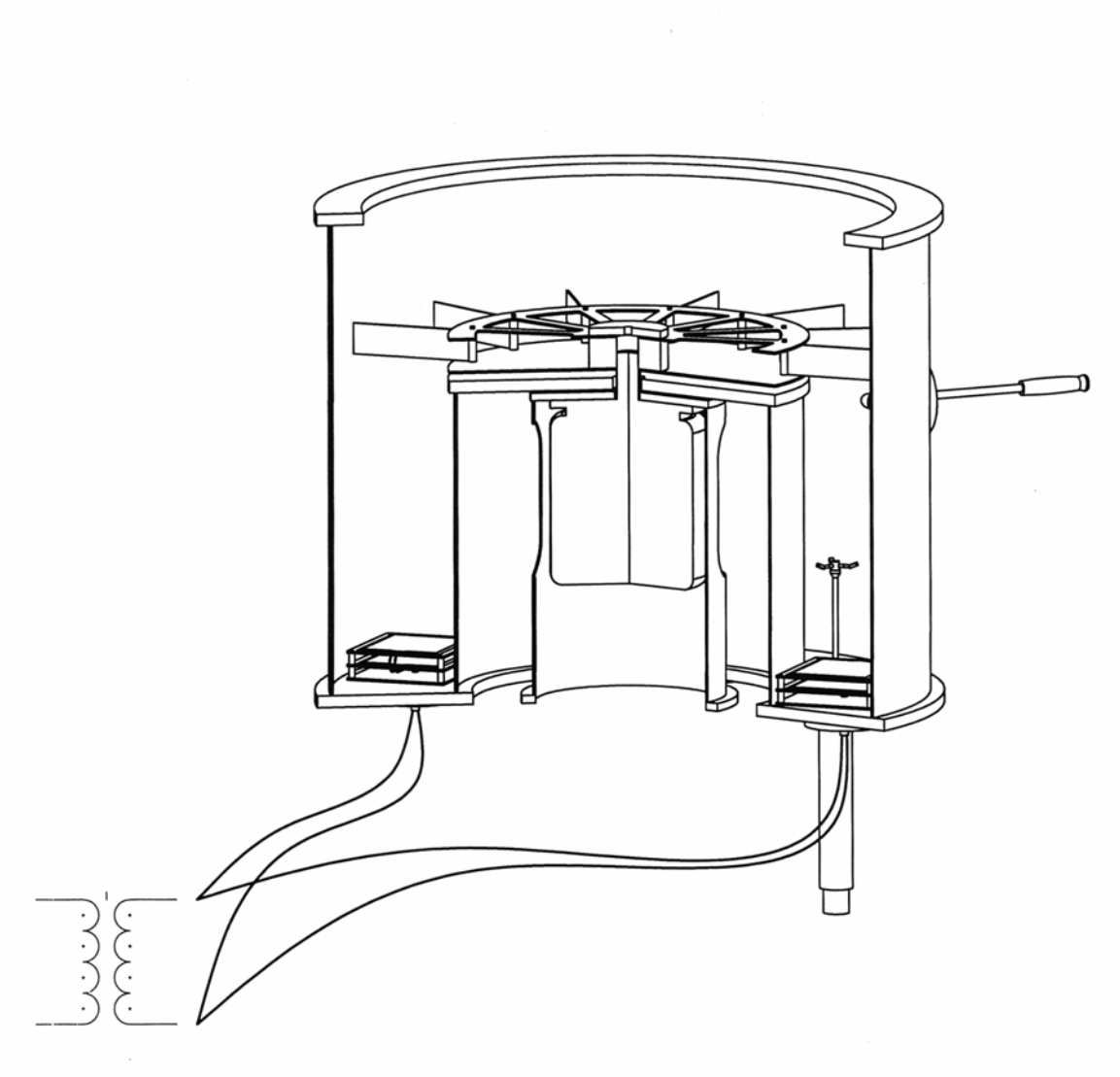

Figure 12: Wind wave tank equipped with heating elements

The electric motor has an efficiency of less than 100% in converting electric power to shaft power, thus the motor heats the surrounding motor case, thereby heating the surrounding water. To solve this, a fan was installed in a duct to ventilate the motor.

6.2 Latent Enthalpy Transfer

The following formulation and analysis shows that for an experiment in which the water and the ambient temperature are equal, the latent enthalpy transfer and the mass transfer coefficients are equal.

The latent enthalpy transfer from the water is:

$$\dot{m}L_{V,w} = C_q V_a A\left(\rho_{sat,w}L_{V,w} - \phi\ \rho_{sat,air}L_{V,air}\right) \tag{31}$$

where $\dot{m}$ is the mass rate of evaporation, $L_{V,w}$ is the latent heat of evaporation at the temperature of the water, $L_{V,air}$ is the latent heat of evaporation at the temperature of the air, C_q is the latent enthalpy transfer coefficient, V_a is the air velocity, A is the water surface area, ϕ is the relative humidity, and $\rho_{sat,w}$ and $\rho_{sat,air}$ are the saturation water vapor density at the water and air temperature respectively.

Because the heating elements keep the water temperature equal to the air temperature, $L_{V,w} = L_{V,air}$ and $\rho_{sat,w} = \rho_{sat,air}$. Therefore, eq. (31) is reduced to give:

$$\dot{m} = C_q V_a A \rho_{sat,w}\left(1 - \phi\ \right) \tag{32}$$

or

$$C_q = \frac{\dot{m}}{V_a A \rho_{sat,w}\left(1 - \phi\ \right)} \tag{33}$$

The last expression for C_q - the latent enthalpy transfer coefficient - is equivalent to the mass transfer coefficient for these specific experimental conditions.

Eq. (32) can also be written as $\frac{dm}{dt} = C_q V_a A \rho_{sat,w}(1-\phi)$. Integrating:

$$\int_0^{m_{tot}} dm = m_{tot} = C_q V_a A \int_0^T \rho_{sat,w}(1-\phi)dt \tag{34}$$

or

$$C_q = \frac{m_{tot}}{V_a A \int_0^T \rho_{sat,w}(1-\phi)dt} \tag{35}$$

where m_{tot} is the total water mass evaporated in a specific experiment. In our procedure, each experiment lasts $n = 1{,}000 - 2{,}000$ min, and $\rho_{sat,w} = \rho_{sat,w}(t)$ and $\phi = \phi(t)$. The temperature and relative humidity (RH) are recorded once per minute.

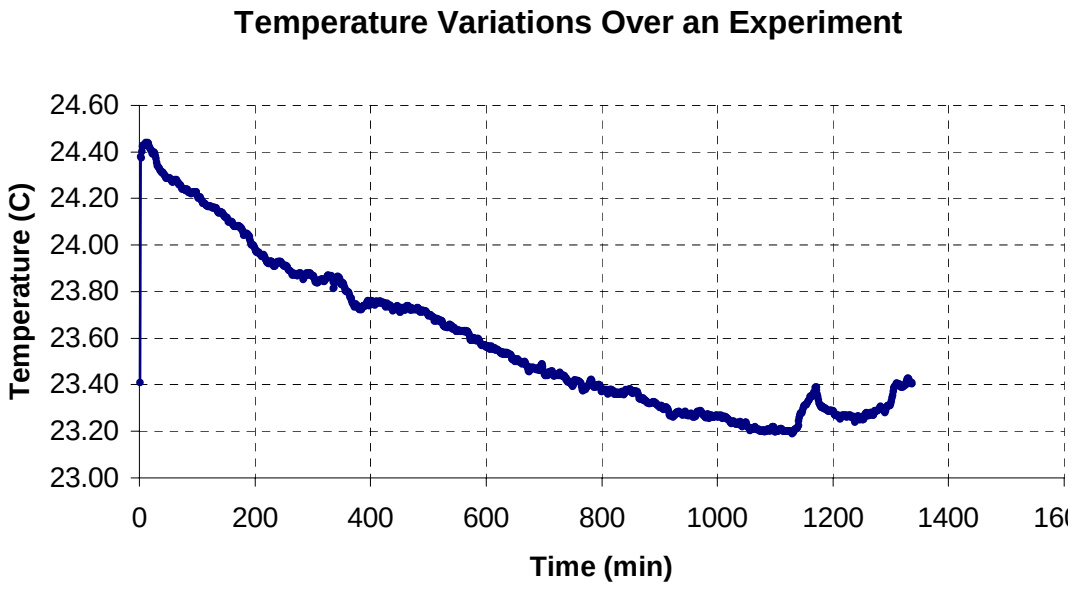

Figure 13: Typical temperature variations over an enthalpy transfer experiment

The integral in (35) is written as a difference form and is performed numerically to give:

$$C_q = \frac{m_{tot}}{V_a A \sum_{1}^{n} \rho_{sat,wi} (1 - \phi_i) \Delta t} \tag{36}$$

In fact, since the heating elements are activated by a temperature difference between the ambient air and water, there are slight temperature differences between the water and room temperature of about 0.3 C, on average. Therefore, equation (36) may be re-written more accurately as:

$$C_q = \frac{m_{tot}}{V_a A \Delta t \sum_{1}^{n} (\rho_{sat,wi} - \phi_i \rho_{sat,air,i})} \tag{37}$$

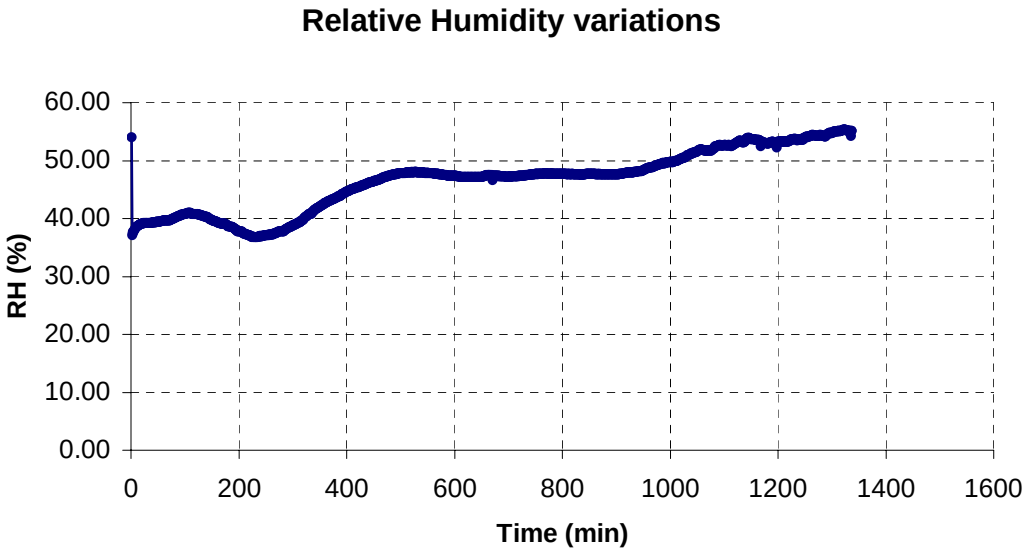

Figure 14: Typical relative humidity variations over an enthalpy transfer experiment.

Since the tank walls are not perfectly circular, the cross sectional area of the tank was measured around the height of the water surface using a known amount of water and measuring its rise using the micrometer. The measured water surface area is $A = 0.4769\ m^2$. Using this and $\Delta t = 60\ sec$ (data recording interval by the spreadsheet) Equation (37), it becomes:

$$C_{q,latent} = 3.495\ 10^{-2} \frac{m_{tot}}{V_a \sum_{1}^{n} (\rho_{sat,wi} - \phi_i \rho_{sat,air,i})} \quad (38)$$

where m_{tot} is the total water mass evaporated in Kg during a specific experiment, V_a is the air speed in m s^{-1}, ϕ_i is the relative humidity each minute. The saturation water vapor pressure at the water surface and in the air as a function of temperature is calculated using the semi-empirical Clausius-Clayperon equation (Ludlam, 1980):

$$P_s = 100 \exp\left[1.8096 + \frac{17.27(T - 273.16)}{(T - 35.86)}\right] \quad (39)$$

where T is the temperature in K. The saturation vapor density is calculated using the ideal gas equation:

$$\rho_{sat} = \frac{P_s}{R_{H_2O} \cdot T} \quad (40)$$

where R_{H_2O} is the gas constant for water vapor. $R_{H_2O} = 461.5 \frac{J}{Kg \cdot K}$

Experiments were performed for 100, 120, 140…..480 RPM. The air velocity for each RPM was measured using the anemometer, and the temperature of the water, ambient air and relative humidity were recorded, enabling the calculation of $\sum_{1}^{n} \left(\rho_{sat,wi} - \phi_i \rho_{sat,air,i}\right)$ for each experiment. A summary of the latent enthalpy transfer coefficient Vs. $V_{0.285}$ is shown in figure 15. $V_{0.285}$ is the air velocity at the height of the anemometer placement, 0.285 m above the water surface.

Previously, the friction velocity vs. $V_{0.285}$ has been found by experiment and therefore, it is possible to calculate enthalpy transfer coefficient normalized with u_* using:

$$C_{q,latent\ U_*} = C_{q,0.285} \cdot \frac{V_{0.285}}{u_*} \quad (41)$$

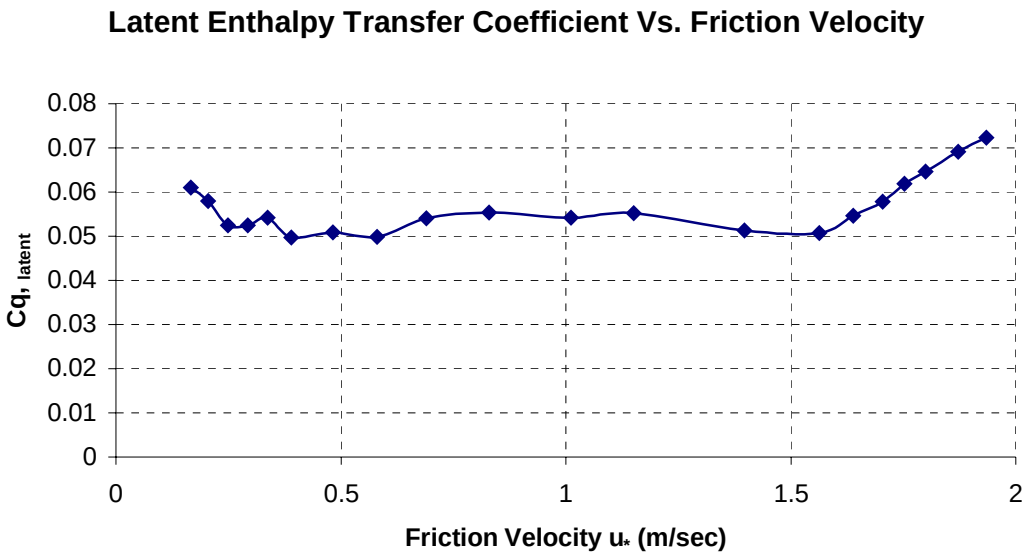

Figure 15: Latent enthalpy transfer coefficient $C_{q,\ latent}$ Vs. u_* - the friction velocity. The coefficient $C_{q,\ latent}$ is normalized with u_*.

The final step is to calculate the latent enthalpy transfer coefficient normalized with U_{10}. For this, it is possible to apply the data of friction velocity vs. the extrapolated wind speed at a height of 10 meters above the water surface that was used to plot Figure 11 and the data of drag coefficient vs. the extrapolated U10 that was used to plot Figure 10.

For convenience, let's denote the latent enthalpy transfer coefficient normalized with the friction velocity as C_{q*} and the latent enthalpy transfer coefficient normalized with U_{10} as C_{q10}. After some calculations it is possible to show that:

$$C_{q10} = C_{q*} \cdot \sqrt{C_{D10}} \qquad (42)$$

Or alternatively:

$$C_{q10} = C_{q*} \cdot \frac{u_*}{U_{10}} \qquad (43)$$

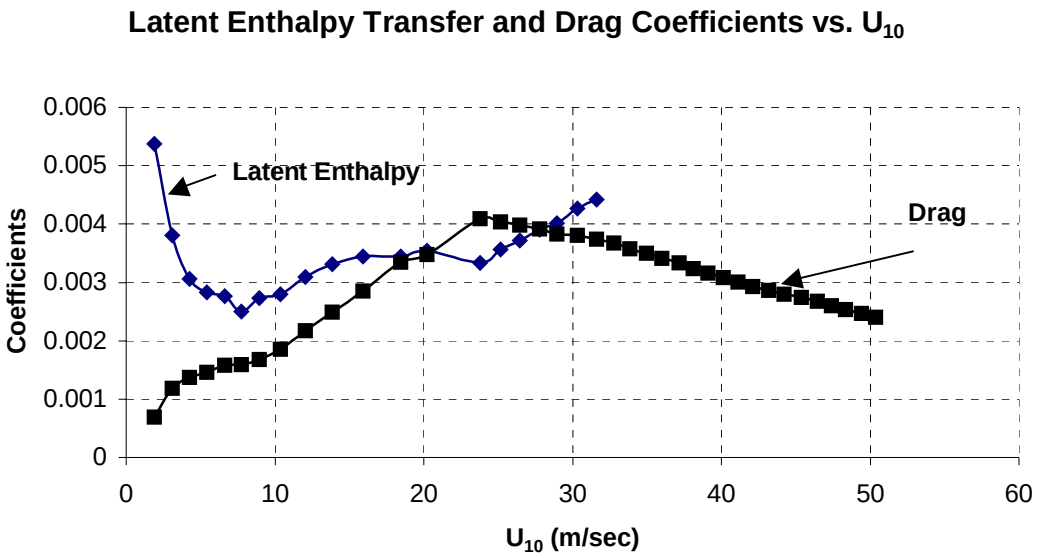

Figure 16: Extrapolation of latent enthalpy transfer and drag coefficients vs. U_{10}.

Unfortunately, in the enthalpy transfer experiments it was impossible to reach high RPM and air speed U_{10} higher than 32 m/sec. This was due to the absence of lid on the tank that caused entrainment of air that added a load on power-limited electric motor.

7. Tank Limitations

A comparison between characteristics of a few experiments was made. Such a comparison is important for identifying the limitations of the apparatus and to design future experiments.

The false bottom is a valuable component of the facility. It can be used to vary the distance from the paddle to the water surface without changing the amount of water in the tank. Unfortunately, the possible height changes implemented by the false bottom are no more than 20 cm owing to the height of the tank.

In further studies it might be useful to consider modifying the wind-wave tank by increasing its height to about 3-5 meters. In such a tank, the false bottom position could be changed by meters rather than centimeters. Also, a tall tank in which the paddle is much higher than the water surface will prevent the water spray from reaching the paddle blades.

At high RPM the water velocity $\mathbf{V_w}$ reached 1.5 - 1.7 m/sec. Owing to the parabolic shape of the water surface (see appendix), the distance from the water surface to the paddle near the outer wall is different from the distance near the inner wall. This difference can reach 15 cm for $V_w \cong 1.7\ m/\sec$. This introduces an error in calculating z_a, the distance from the water surface to the paddle and to the anemometer that measures the air speed. The highly parabolic water surface for high RPM also alters the moment of inertia of the water mass, and this introduces an error in the calculation of the shear stress.

It was also observed that at a paddle RPM that corresponds to $U_{10} \cong 30\ m/\sec$ and higher, water spray is generated, especially when the lid is on. It is estimated that the centrifugal acceleration of the spray is on the order of $100 - 200\ m/\sec^2$ so that its flight time scale before impacting the tank walls is about 0.1 sec. This point may explain the declining C_D for $U_{10} > 25\ m/\sec$ and should be the subject of further investigation. The enthalpy transfer experiments seem to provide useful and accurate information as far as the latent enthalpy transfer is concerned. However, the tank air inflow and outflow govern the sensible heat transfer, and this flow pattern in our experiment does not resemble conditions over the ocean. In addition, at high RPM, mechanical dissipation in the air above the water surface and on the tank walls might contribute to sensible heat transfer into the water.

8. Conclusions

The scientific goal of this experimental study is to develop an experimental procedure for estimating air-sea heat and momentum exchange at very high wind speeds, and to present results for these fluxes in a relatively simple apparatus. While the limitations of the circular tank make comparisons to nature problematic, we observe several

interesting features of the results that are consistent with other experiments. Our drag experimental results are consistent with those of Donealn (2004) who used momentum budget showing a steep increase in the drag coefficient up to a wind speed of 25-30 m/sec and then leveling and a decrease of the drag coefficient for a wind speed higher than 30 m/sec. This steep increase and leveling of the drag coefficient is also consistent with recent deductions from dropwindsondes deployed in hurricanes Powell (2003), although the highest C_D in Donealn's work is 2.5 10^{-3} while our is 4.0 10^{-3} for air speed of 25-30 m/sec. All of this recent research seems to suggest that the well documented increase in the surface drag coefficient with wind speed over the ocean does not continue indefinitely but levels off at 10 m winds speeds of about marginal hurricane force, and may even decrease at yet higher speeds. Consistent with the abovementioned research, we observe such a decrease in the tank, but this decrease may result from the centrifuging of spray before it can extract momentum from the airflow. We hope to apply some of the estimation techniques described here in future experiments using linear wind-wave flumes.

We also present quantitative estimates of the surface latent enthalpy exchange coefficient at near hurricane wind speeds. The tank limitations did nit enable us to conduct investigation into the sensible enthalpy exchange coefficient. The tank limitations suggest caution in extrapolating these results to nature, they do suggest that the enthalpy coefficient also increases with wind speed, but levels off near marginal hurricane strength. The near equality of the enthalpy and momentum exchange coefficients is consistent with what is required for quantitatively accurate forecasts of hurricane intensity using numerical models (Emanuel, 1995). We hope to apply some of the same experimental procedures developed here to deduce enthalpy fluxes in larger, linear wind-wave flumes.

Acknowledgment:

The authors wish to thank the MIT Edgerly Fund for providing the funding for the wind wave tank construction and to Peter Morley and David Bono for their technical assistance.

References:

Alamaro, M.; "Wind Wave Tank for the Investigation of Momentum and Enthalpy Transfer from the Ocean Surface at High Wind Speed," Master thesis at the Department of Earth, Atmospheric and Planetary Sciences, Massachusetts Institute of May, 2001. See also: http://web.mit.edu/hurricanelab/ThesisWebsite.pdf

Bistre, M. and Emanuel, K.A., 1998: Dissipative heating and hurricane intensity. *Meteoric. Atoms*. Physic. **65**, 233-240.

Donelan, M.A. et al 2004: On the Limiting Aerodynamic Roughness of the Ocean in Very Strong Winds. Forthcoming in *Geophysical Research Letters.*

Emanuel, K.A., 1986: An air-sea interaction theory for tropical cyclones. Part I. *J. Atmos. Sci*., **42**, 1062-1071.

Emanuel, K.A., 1988: The maximum intensity of hurricanes. *J. Atmos. Sci*., **45**, 1143-1155.

Emanuel, K.A., 1995: Sensitivity of tropical cyclones to surface exchange coefficients and a revised steady-state model incorporating eye dynamics. *J. Atmos. Sci.*, **52**, 3969-3976.

Fox, R.W, and McDonald, A.T. 1998: *Introduction to Fluid Mechanics*. John Wiley & Sons, Inc., New York.

Geerneart, G. L., S. E. Larsen and F. Hansen, 1987: Measurements of the wind stress, heat flux and turbulence intensity during storm conditions over the North Sea. *J. Geophys. Res.*, **92**,13127-13139.

Ludlam, F.H., "Clouds and storms; the behavior and effect of water in the atmosphere," The Pennsylvania State University Press, 1980.

Ooyama, K., 1969: Numerical simulation of the life cycle of tropical cyclones. J. Atmos. Sci., 26, 3-40.

Powell, M.D, et al 2003: Reduced Drag Coefficient for High Wind Speeds in Tropical Cyclones. *Nature*, Vol. 422, 279-283.

Rosenthal, S. L., and M. S. Moss, 1971: Numerical experiments of relevance to Project STORMFURY. NOAA Tech. Memo. ERL NHRL-95, Coral Gables, FL, 52 pp.

Appendix: Parabolic Shape Factors of the water surface

Due to the centrifugal acceleration, the water surface will not be horizontal. The water surface becomes parabolic in r or $H = H(r)$. Therefore, the definition of z_a, the height above the water surface where air velocity is measured is compromised. The water surface area and the water moment of inertia are also changed.

Consider rigid body rotation of the water mass. Equilibrium in the r direction at any point in the water gives:

$$\frac{dp}{dr} = -\rho\frac{V^2}{r} = -\rho\,\Omega^2\,r \quad \text{or} \quad \frac{dp}{dr} = \frac{dp}{dz}\frac{dz}{dr} = -\rho\,g\frac{dz}{dr} = -\rho\,\Omega^{\,2}r \tag{a1}$$

Integrating gives:

$$\Delta z(r) = \frac{\Omega^2}{2g}\left(r^2 - r_{in}^2\right) \qquad r \geq r_{in} \tag{a2}$$

Using $\Omega = \frac{V_w}{R_D}$ and substituting the values for R_D, r_0 and r_{in}, equation (a1) provides the height difference of the water surface between the outer water and inner walls for the specific geometry of the tank:

$$\Delta z = 0.0528\,V_w^2 \tag{a3}$$

Where V_w is in m s^{-1}

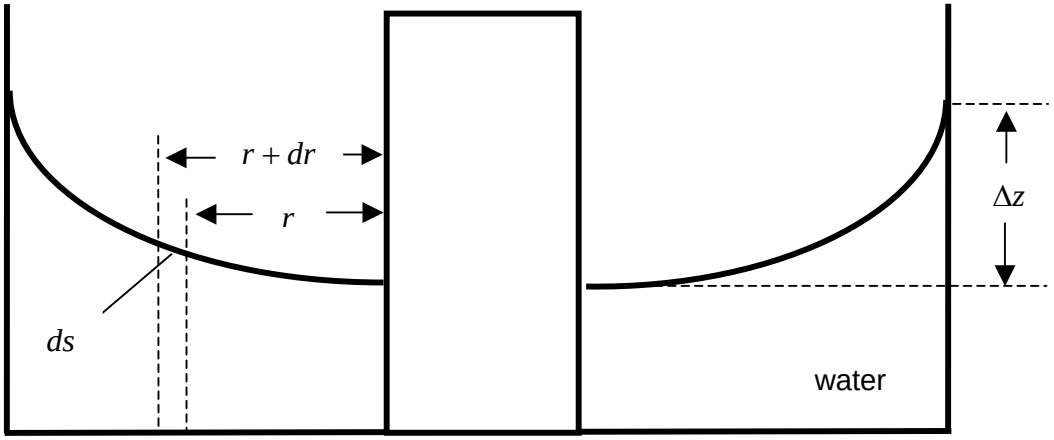

Figure a1: Parabolic surface of rotating rigid body water mass

The differential surface area in the rotating system is:

$$dA = ds\ 2\pi\ r \quad \text{or} \quad A(r) = 2\pi \int_{r_{in}}^{r_0} r\ ds \tag{a4}$$

Where:

$$ds = \sqrt{1+\left(\frac{dz}{dr}\right)^2}\ dr \quad \text{and (a1) becomes:} \quad \frac{dz}{dr} = \frac{\Omega^2}{g} r$$

(a5)

Substituting and integrating:

$$A(r) = 2\pi \cdot \frac{g^2}{3\Omega^4} \cdot \left[\left(1+\frac{\Omega^4}{g^2} r^2\right)^{\frac{3}{2}} - \left(1+\frac{\Omega^4}{g^2} r_{in}^2\right)^{\frac{3}{2}}\right] \tag{a6}$$

The parabolic area factor $PF_{area} = \frac{A(r_0)}{A_0}$ is the ratio of the new water surface area to the area of the surface without rotation and is obtained by substituting $r = r_0$ and $\Omega = \frac{V_w}{R_D}$ in equation (a6) so:

$$PF_{area} = \frac{2\pi \cdot \frac{g^2}{3\Omega^4} \cdot \left[\left(1 + \frac{\Omega^4}{g^2} r_0^{\,2} \right)^{\frac{3}{2}} - \left(1 + \frac{\Omega^4}{g^2} r_{in}^2 \right)^{\frac{3}{2}} \right]}{\pi \left(r_0^2 - r_0^2 \right)} \qquad \text{(a7)}$$

After substituting the apparatus dimensions and simplifying, the parabolic area factor become:

$$PF_{area} = 8.879 \frac{\cdot \left[\left(1 + 0.11578\, V_w^4 \right)^{\frac{3}{2}} - \left(1 + 0.0407\, V_w^4 \right)^{\frac{3}{2}} \right]}{V_w^4} \qquad \text{(a8)}$$

where V_w is the water velocity in m s^{-1}. The increase in surface area due to rotation of the water will be used to obtain the exchange rates per unit surface area.

Similarly, an analysis has been made to define a parabolic torque correction factor for the shear stress that propels the rotational water motion. The basic assumption is that the shear stress over the water surface is not a function of the distance from the tank center or that $\tau_s \neq \tau_s(r)$. However, since the shear stress now is over a parabolic surface, let's denote the stress as τ_{pf} (where the ***pf*** stand for parabolic factor). The stress τ_{pf} acts on a differential surface area $2\pi\, r \cdot ds$ and the differential torque generated by the stress at a radial distance r is:

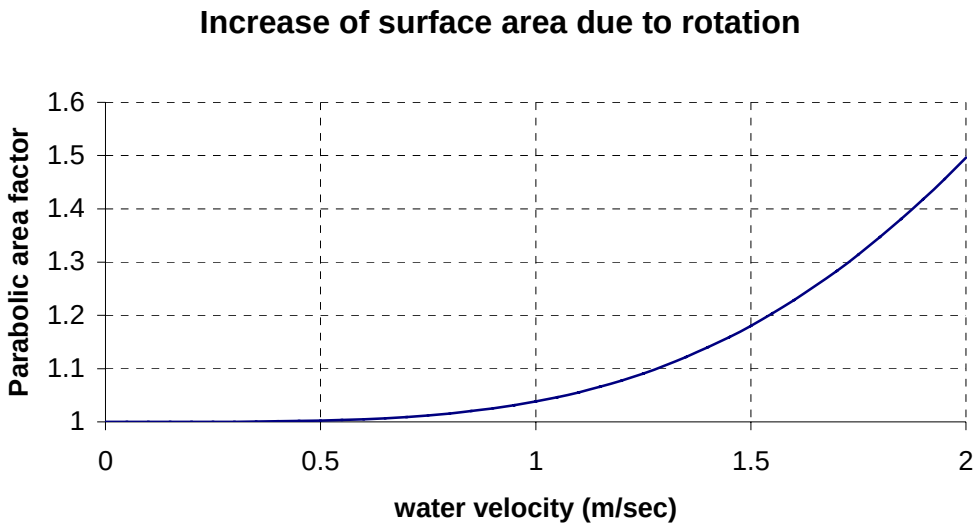

Figure a2: The ratio of the surface area due to rotation to the surface area without rotation as a function of the water velocity at the sonic Doppler location.

$$dT_{pf} = \tau_{pf}(2\pi\, rds)r = \tau_{pf} 2\pi\, r^2 ds = \tau_{pf} 2\pi\, r^2 \sqrt{1+\left(\frac{dz}{dr}\right)^2}\; dr \qquad \text{(a9)}$$

The solutions for τ_{pf} becomes (Alamaro 2001):

$$\tau_{pf} = \left[\frac{\frac{2}{3}\pi\left(r_0^3 - r_{in}^3\right)}{2\pi \int_{r_{in}}^{r_0} r^2 \sqrt{1+\left(\frac{V_w^4}{R_D^4 g^2}\right) r^2}\; dr} \right] \cdot \tau_s = \frac{\tau_s}{PF_{torque}} \qquad \text{(a10)}$$

In equation (a10) the term in the bracket is a correction factor for the shear stress over a parabolic water surface. Substituting the actual values for the apparatus dimensions r_0, r_{in}, R_D, and g we get:

$$PF_{torque} = 34.48 \int_{r_{in}}^{r_{out}} r^2 \sqrt{1+0.504\, V_w^4\, r^2}\; dr \qquad \text{(a11)}$$

The explicit expression for the solution of equation (a11) is a long and cumbersome expression. Therefore, the integral in (a11) has been solved numerically for $\mathbf{0} < V_w < \mathbf{2}\ \ m/\sec$. Curve fitting has been performed with a sixth degree polynomial to obtain a working formula for the torque parabolic factor as a function of the water velocity.

The shear stress for the rotating water mass in the wind wave tank is obtained by combining equations (13) and (a11) and by using the dimensions of the tank to obtain:

$$\tau_{pf} = \frac{-1050 \cdot H \cdot \frac{\partial V_w}{\partial t}}{PF_{torque}} \qquad \text{(a12)}$$

Where H is the water depth.

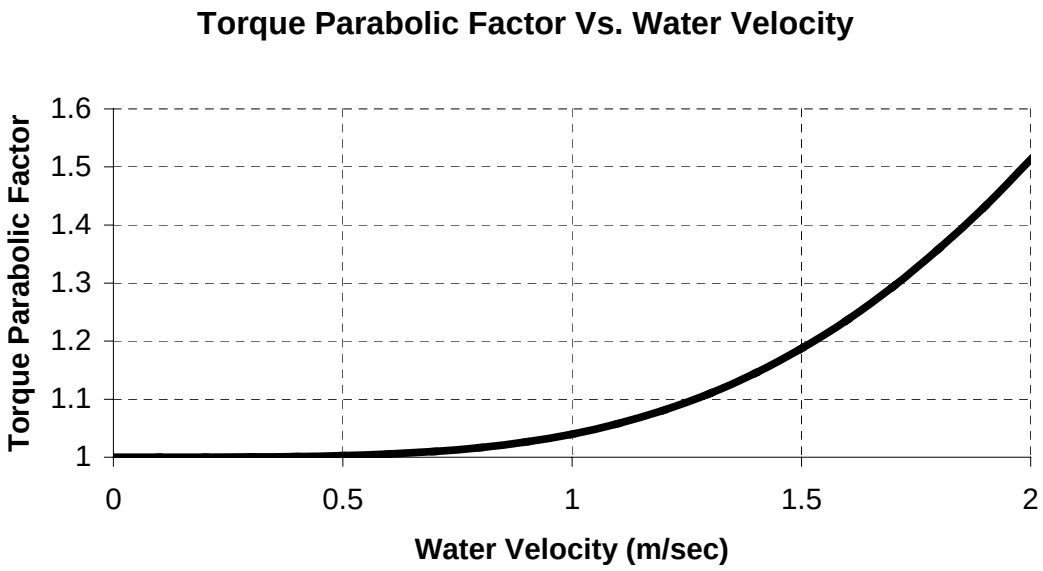

Figure a3: The correction factor to the propelling shear stress as a function of water velocity at the radial location of the ADV.